Validation Assessment of Loci/GGFS Gas Granular Flow Solver Predictions of Ejecta from Physics Focused Ground Test

Andrew B. Weaver[1], Thomas P. Shurtz[2]
Jacobs Space Exploration Group, NASA Marshall Space Flight Center, Huntsville, AL, 35808, USA

Peter A. Liever[3]
CFD Research Corporation, Jacobs Space Exploration Group, NASA Marshall Space Flight Center, Huntsville, AL, 35808, USA

Jeffrey S. West[4]
NASA Marshall Space Flight Center, Huntsville, AL, 35808, USA

NASA is preparing to return humans to the Moon to establish a sustained Lunar presence through the Artemis program. One area of concern for Lunar landers is the plume surface interaction (PSI) environment that poses several risks during a propulsive landing. Understanding the PSI environment caused by the landers is therefore important to designing successful landing missions. Towards this end, a two-phase, gas granular flow solver, Loci/GGFS, has been developed to predict the cratering and ejecta physics expected during a Lunar landing. The focus of this paper is on a validation assessment of Loci/GGFS predictions of ejecta with monodisperse glass beads (MGB). The validation assessment is performed with respect to the Physics Focused Ground Test 1 (PFGT1) conducted at NASA Marshall Space Flight Center (MSFC) in 2021. It is found that Loci/GGFS predicts similar initial cratering and ejecta features, with predictions of average velocities that are within 25% of experimental values.

I. Nomenclature

alpha	=	*solid volume fraction*
D_e	=	nozzle exit diameter
h	=	initial nozzle height above regolith simulant
M_e	=	Mach number at nozzle exit
$\dot{m}$	=	nozzle mass flow rate
MGB	=	monodisperse glass beads
PFGT1	=	physics focused ground test 1

[1] Senior Engineer, Sev1Tech, and AIAA Senior Member
[2] Fluid Dynamicist, Jacobs
[3] Technical Fellow, CFD Research Corporation, AIAA Associate Fellow
[4] AST, MSFC Fluid Dynamics Branch, AIAA Senior Member

II. Introduction

Numerous crewed and uncrewed Lunar landing missions are planned with the use of propulsive systems to control the descent to the Moon's surface. Each of these landings are expected to encounter plume surface interaction (PSI) effects based on current understanding of PSI and observations from past landings such as the Apollo Lunar Module, Intuitive Machines Nova-C lander, and InSight robotic Mars Lander. These PSI effects include cratering and ejecta that pose multiple risks to the lander and nearby assets: (1) landing on sloped surface causing excessive vehicle tilt, (2) high-speed ejecta/debris impacts to the vehicle or nearby assets driven by plume flow, and (3) view obscuration of the surface below due to regolith particle ejecta. Modeling and simulation of PSI physics will be essential to support the mitigation of PSI related risks.

A two-phase, gas granular flow solver, Loci/GGFS,[1] was developed to model the complex, gas/solid interaction between an impinging gas flow with solid, granular media expected to be encountered on extra-terrestrial soils. Loci/GGFS treats both gas and solid phases with an Eulerian modeling approach, which allows for the simulation of dense, solid phase flows in real applications that would be prohibitively expensive with a Lagrangian particle tracking approach. Multiple closure models are implemented into Loci/GGFS to describe the particle-particle and particle-fluid interactions, such as drag models that are relevant to ejecta modeling.[2]

To validate model predictions of plume impingement, cratering, and ejecta, a series of ground tests known as the Physics Focused Ground Test (PFGT) were performed over a range of nozzle gas and soil conditions relevant to Lunar and Martian landings.[3] The focus of this paper is on the validation assessment of Loci/GGFS with respect to ejecta measurements from two select tests from PFGT: (1) R142 and (2) R139. These tests correspond to Martian-like and Lunar-like ambient atmosphere conditions, respectively, with monodisperse glass beads (MGB) as the soil simulant in the soil bin. Thus, Loci/GGFS is validated for ejecta against PFGT tests operating in different cratering regimes.

In this paper, the validation of ejecta predictions from Loci/GGFS will be assessed with respect to two tests from PFGT that exhibit signs of two distinct cratering regimes. The experimental and computational setups for each test and corresponding simulation will be described, and comparisons of ejecta locations and velocities over time will be reported. This validation assessment is part of an initial, phase I validation effort to assess the current modeling status, with follow-on phase validations planned to establish modeling best practices and identification of any potential model development needs to further reduce modeling related uncertainties.

III. Experimental Setup

The PFGT1 test series performed at NASA MSFC explored nozzle plume, vacuum chamber, and soil condition parameter space to capture relevant physics for Lunar and Martian PSI.[3][4] The test included a nozzle test assembly that was centered above a splitter plate designed to split the nozzle flow in half, such that half of the flow impinged on the 80 cm x 40 cm x 30 cm soil bin and half flowed outside of the soil bin. A transparent, acrylic viewing pane was used along with the splitter plate so that the cratering process could be observed during the test. This experimental test setup is illustrated in Fig. 1 below.

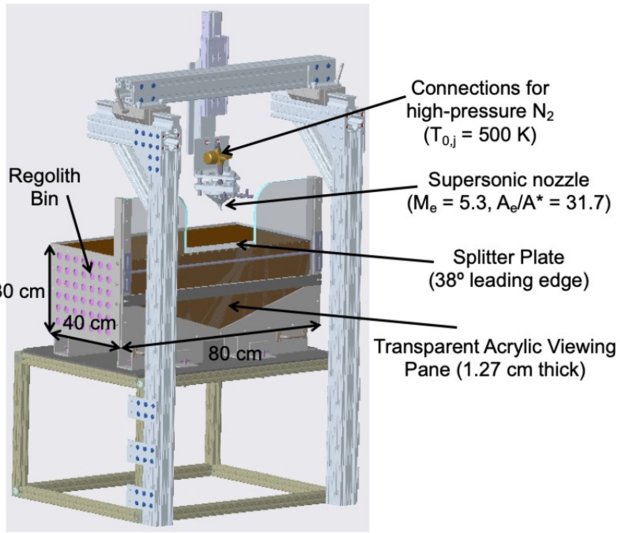

Fig. 1 PFGT1 experimental setup with nozzle test assembly, support structure, and soil bin [4]

The two tests selected for validation are R142 and R139. Both tests are performed using MGB soil simulant, but the nozzle flow rates, nozzle heights, and ambient pressures in the vacuum chamber differ. R142 was tested with a nominal mass flow rate of 8.6 g/s at a nondimensional nozzle height of ten and an ambient pressure of 4.5 Torr, while R139 was tested with a lower, nominal mass flow rate of 0.32 g/s at a nondimensional nozzle height of 8 and an ambient pressure of 0.02 Torr. These testing conditions are summarized in Table 1 below.

Table 1 Nominal test conditions for selected PFGT1 tests for validation of Loci/GGFS predictions of ejecta

PFGT1 Run #	Soil Simulant	Particle Diameter (micron)	P_{chamber} (Torr)	h/D_e	Mass Flow Rate (g/s)
R139	MGB	150	0.02	8	0.32
R142	MGB	150	4.5	10	8.6

A high-speed camera is used in PFGT1 to image the ejecta along the transparent viewing pane.[3][5] The high frame rate of the camera allows for accurate tracking of individual particles, from which particle locations and velocities can be obtained.[6] The field of view for the ejecta camera spans approximately 9 cm wide by 5 cm high near the edge of the splitter plate, as illustrated in Fig. 2. Ejecta camera images from R142 and R139 are shown in Fig. 3 at times of 0.13 s and 0.38 s as an example of the available data. Thus, comparisons between Loci/GGFS predictions of ejecta and measured ejecta are with respect to the indicated field of view near the edge of the splitter plate.

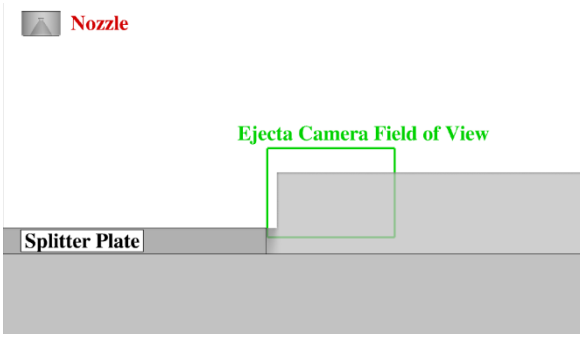

Fig. 2 High-speed ejecta camera field of view for PFGT1 tests [3][5]

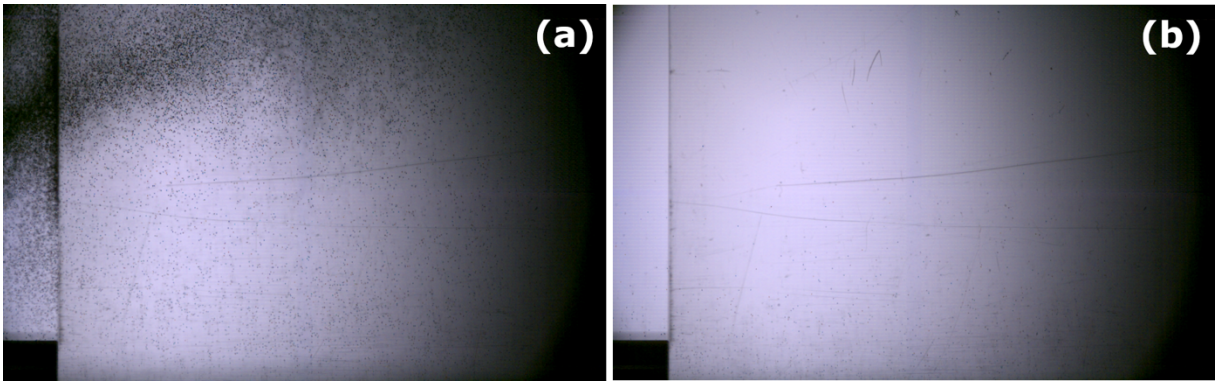

Fig. 3 High-speed ejecta camera images from (a) R142 at 0.13 s and (b) PFT1_R139 at 0.38 s

IV. Computational Setup

Time-dependent simulations of PFGT1 tests are performed using Loci/GGFS with a 3D geometry, as illustrated in Fig. 4. Apart from the nozzle height above the initial regolith location, the computational geometries for R142 and R139 were the same. Pressures within the vacuum chamber are maintained at the nominal pressures indicated in Table 1 for each PFGT1 test via outflow boundary conditions applied to the farfield boundaries shown in Fig. 4. The vacuum chamber pressures do not increase much during the short time period for which processed ejecta data exists; therefore assuming constant pressure at the farfield boundary is expected to have negligible impacts on the plume surface interaction predictions.

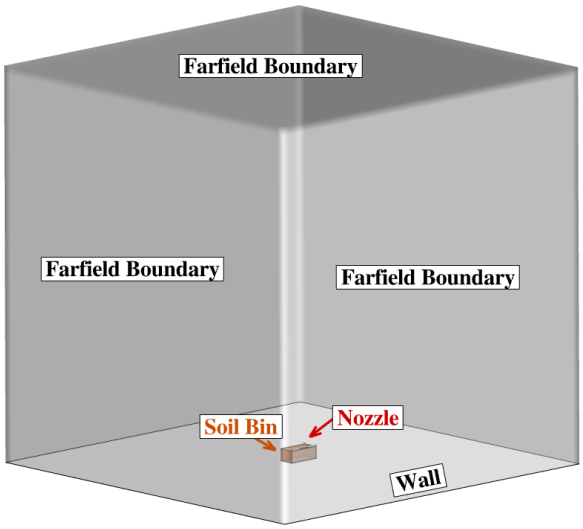

Fig. 4 Modeled PFGT1 geometry in Loci/GGFS simulations

It can be observed from Fig. 5 that the entire soil bin is modeled along with the nozzle. The nozzle inflow boundary is in the plenum upstream of the nozzle throat, as indicated by the shaded green boundary in Fig. 5.

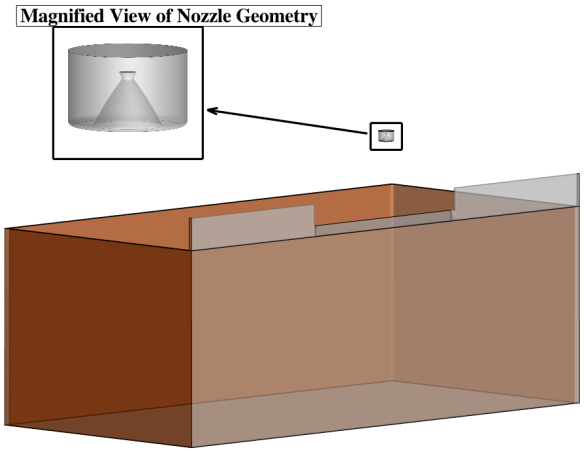

Fig. 5 Modeled nozzle and soil bin geometries in Loci/GGFS simulations of PFGT1

A baseline mesh of approximately 15 million cells is used in the Loci/GGFS simulation of R142, with a cell edge length of 1.5 mm in a region of soil that lies within a 15 cm radius of the nozzle centerline. An illustration of the baseline computational meshes is provided in Fig. 6. An adaptive mesh refinement (AMR) algorithm based on gas velocity and solid volume fraction error is used within Loci/GGFS to refine and coarsen cells located within 11 cm of

the nozzle centerline to a target cell edge length of 500 microns. A similar mesh with 20 million cells initially is used in the Loci/GGFS simulation of R139.

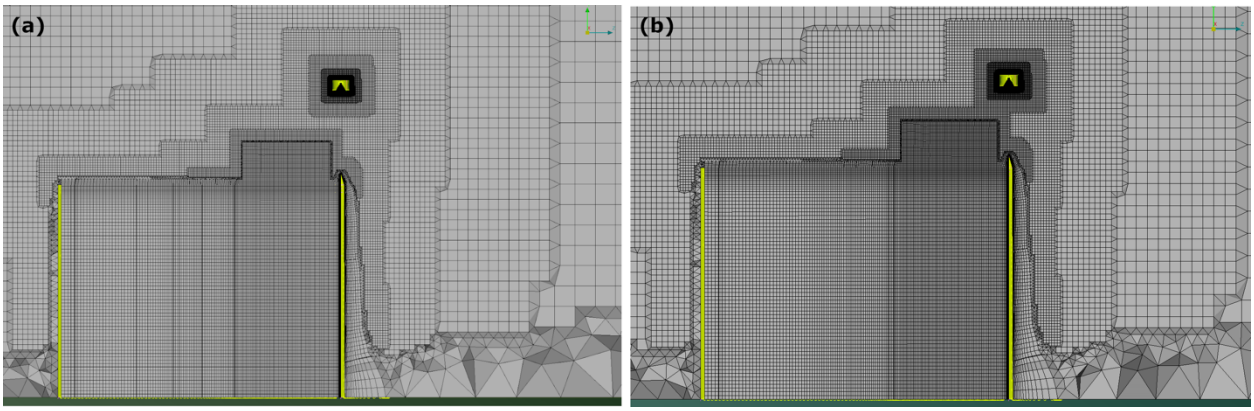

Fig. 6 Illustration of baseline computational meshes used in simulations for (a) R142 and (b) R139

The nitrogen gas plume flow is modeled with temperature-dependent transport properties based on data from NIST,[7] and the plume flow is modeled without a turbulence model. The soda lime soil particles are modeled with 2500 kg/m^3 particle density and a particle diameter of 151 microns.

Due to the transient nature of the PFGT1 tests and the duration of available, processed ejecta data,[6] it is important to use a time-dependent inflow boundary condition. This time-dependent boundary condition comes from high-speed dynamic pressure measurements in the nozzle plenum for each simulated test, and the specified mass flow rates over time are shown in Fig. 7 for each test below.

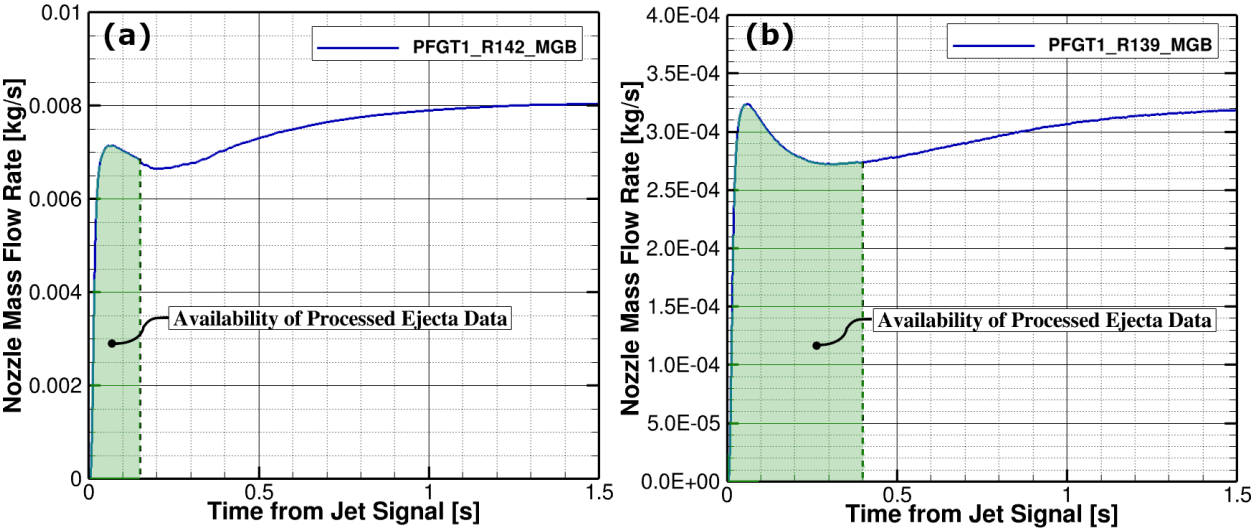

Fig. 7 Transient nozzle mass flow rates in Loci/GGFS simulations of (a) R142 and (b) R139

V. Validation Assessment of Loci/GGFS Ejecta Predictions Against PFGT1 Data

This section details the ejecta predictions from Loci/GGFS simulations of R142 and R139. Significant ejecta features will be identified and compared between Loci/GGFS predictions and test imagery for qualitative validation. Ejecta locations and velocities will also be compared over the early time periods from the tests for which processed ejecta data is currently available.[6] Spatially averaged velocity magnitudes and angles over the ejecta camera field of view, as well as maximum velocity magnitudes will be compared between Loci/GGFS and experimental

measurements. This will allow for comparison between predictions from an Eulerian-based model and measurements from a particle tracking algorithm.

The field-of-view averaged ejecta velocities as a function of time are evaluated for both the processed ejecta and Loci/GGFS simulations as follows. Measured ejecta velocities correspond to individual particles, and therefore the field-of-view averaged ejecta velocity magnitudes are obtained as

$$\boldsymbol{v}_{\mathbf{avg}} = \frac{\mathbf{1}}{\boldsymbol{N}} \sum_{\boldsymbol{i}=\mathbf{1}}^{\boldsymbol{N}} |\vec{\boldsymbol{v}}_{\boldsymbol{i}}| \ , \tag{1}$$

where N is the total number of particles within the ejecta camera field of view at a given point in time. Field-of-view averaged ejecta velocity angles from the ejecta measurements are similarly obtained from the sum of individual particle velocity angles. Since Loci/GGFS is an Eulerian-based model for both the gas and solid phases, field-of-view averaged ejecta velocities are evaluated using the solid volume fraction.

Instead of summing ejecta velocity magnitudes of all particles within the ejecta camera field of view (since individual particles are not simulated in Loci/GGFS), field-of-view averaged ejecta velocity magnitudes are obtained using solid phase volume as the weighting function. Thus, the field-of-view averaged ejecta velocity magnitude from Loci/GGFS is expressed as

$$\boldsymbol{v}_{\mathbf{avg}} = \frac{\sum_{\boldsymbol{i}=\mathbf{1}}^{\boldsymbol{N}_{\mathbf{cell}}} \boldsymbol{\alpha}_{\boldsymbol{i}} \boldsymbol{V}_{\boldsymbol{i}} |\vec{\boldsymbol{v}}_{\boldsymbol{i}}|}{\sum_{\boldsymbol{i}=\mathbf{1}}^{\boldsymbol{N}_{\mathbf{cell}}} \boldsymbol{\alpha}_{\boldsymbol{i}} \boldsymbol{V}_{\boldsymbol{i}}} \ , \tag{2}$$

where α_i is the solid volume fraction within the i-th computational cell, V_i is the cell volume within the i-th computational cell, and N_{cell} is the number of computational cells within the ejecta camera field of view. Field-of-view averaged ejecta velocity angles from Loci/GGFS are similarly obtained using the solid phase volume as a weighting function.

A. R142

The plume from R142 is more collimated and begins to crater immediately. This can be observed from the Mach and solid volume fraction (alpha) contours shown in Fig. 8. There is an initial wave of ejecta flowing radially outward towards the edge of the splitter plate. This ejecta is observed to reach the edge of the splitter plate near the same time of 0.05 s in both the experiment and Loci/GGFS in Fig. 9. As the plume impinges on the MGB soil simulant below, a significant crater begins to form, and a dense wave of ejecta is observed. This dense wave of ejecta is observed in both the experiment and Loci/GGFS, and it is moving radially outwards towards the edge of the splitter plate.

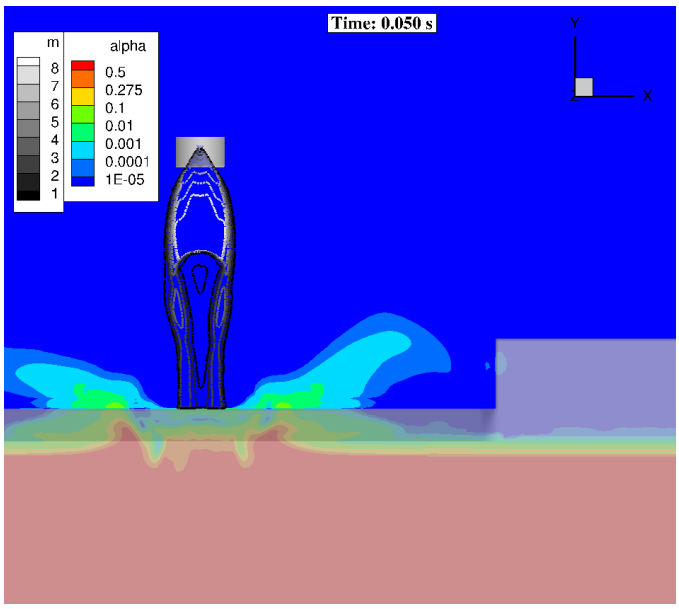

Fig. 8 Mach and solid volume fraction (alpha) contours near splitter plate for R142 at 0.05 s

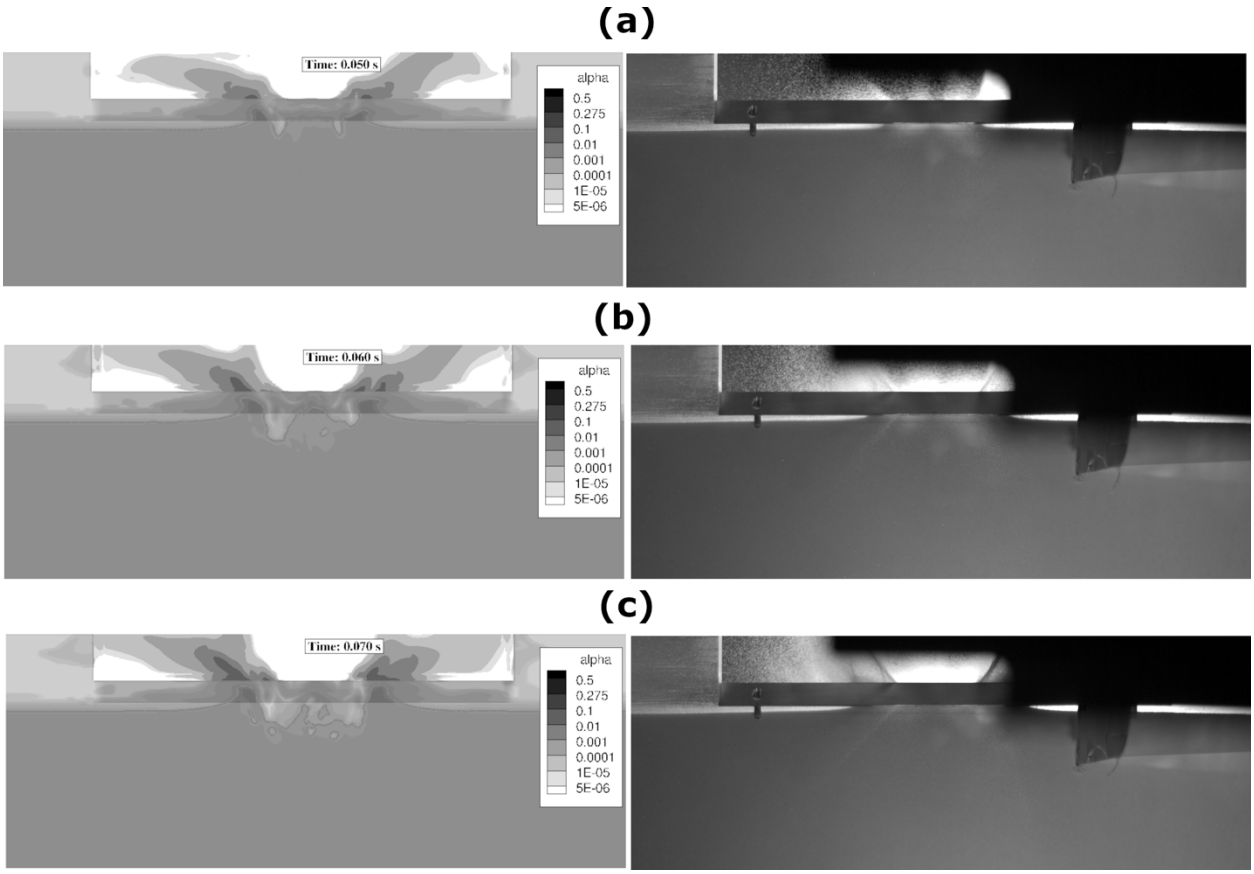

Fig. 9 Comparison of ejecta between Loci/GGFS (left images) and crater camera (right images) at times: (a) 0.05 s, (b) 0.06 s, (c) 0.07 s. Loci/GGFS images show alpha contours on slice near splitter plate

Multiple, similar ejecta features are identifiable between Loci/GGFS predictions and experimental images between the times of 0.08 s and 0.13 s in Fig. 10. Ejecta emanating from the sides of the crater walls continues to darken, indicating denser concentrations of ejecta. This can be observed from the crater camera images in Fig. 10 for R142. The solid volume fraction (alpha) in Loci/GGFS shows similar increases in particle concentrations from the sides of the crater walls and moving upwards above the splitter plate. Denser streams of ejecta appear to cross the side of the splitter plate after 0.1 s in both Loci/GGFS predictions and experimental images. Also, note the "V"-shaped ejecta pattern in the experimental image near the left side of the crater and emanating above the splitter plate. A similar

pattern is visible in Loci/GGFS predictions, and it occurs as ejecta impinges on the splitter plate. Refer to Fig. 11 for annotated images indicating the “V”-shaped pattern of discussion at 0.13 s.

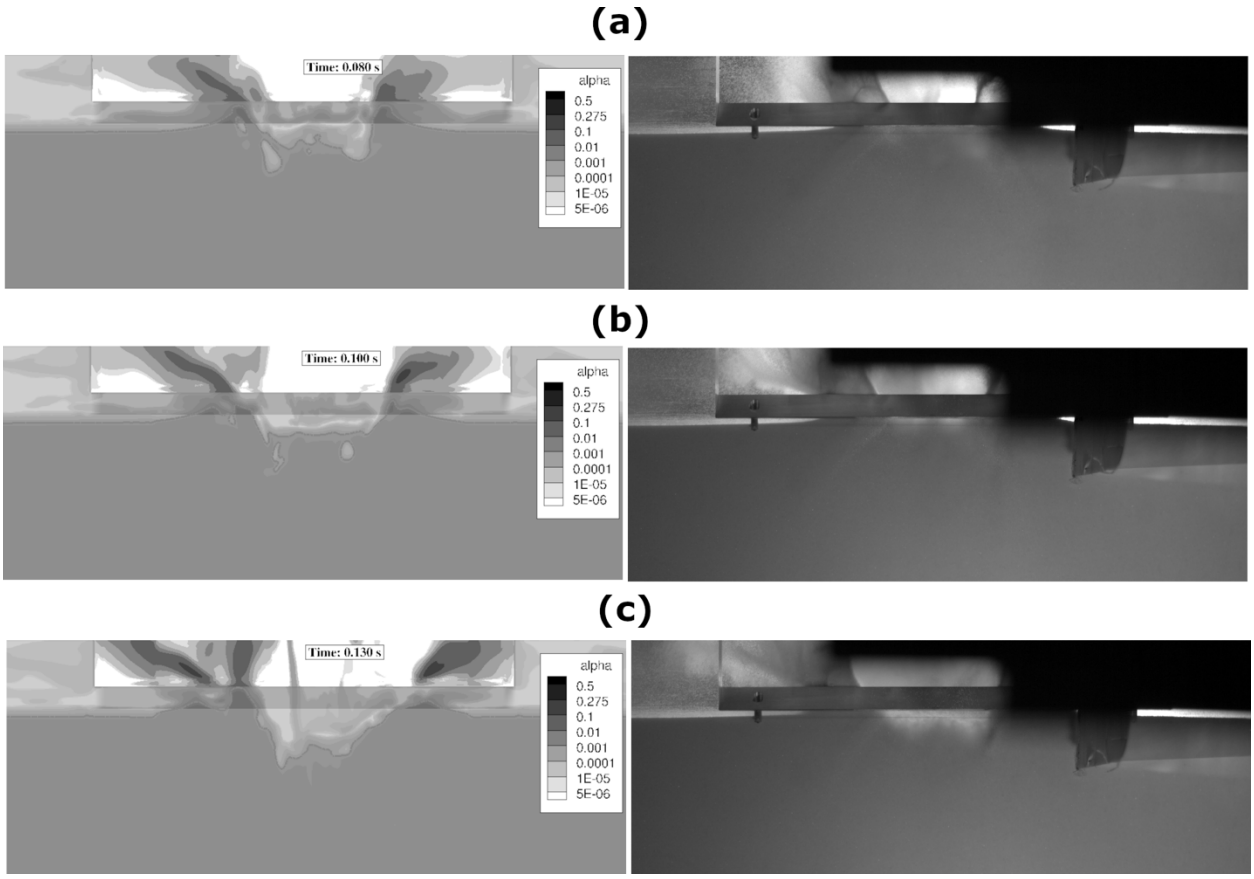

Fig. 10 Comparison of ejecta between Loci/GGFS (left images) and crater camera (right images) at times: (a) 0.08 s, (b) 0.1 s, (c) 0.13 s. Loci/GGFS images show alpha contours on slice near splitter plate

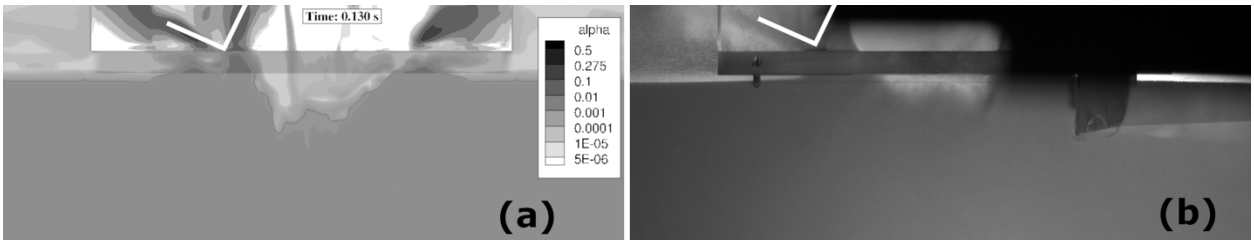

Fig. 11 Comparison of "V"-shaped ejecta pattern between (a) Loci/GGFS and (b) crater camera images at 0.13 s. Annotated feature shown in white lines

Average velocity magnitudes, average velocity angles, and maximum velocity magnitudes are shown as a function of time for both ejecta measurements and Loci/GGFS predictions in Fig. 12. The average velocities from measurements are obtained from Eq. (1), and average velocities from Loci/GGFS are obtained from Eq. (2).

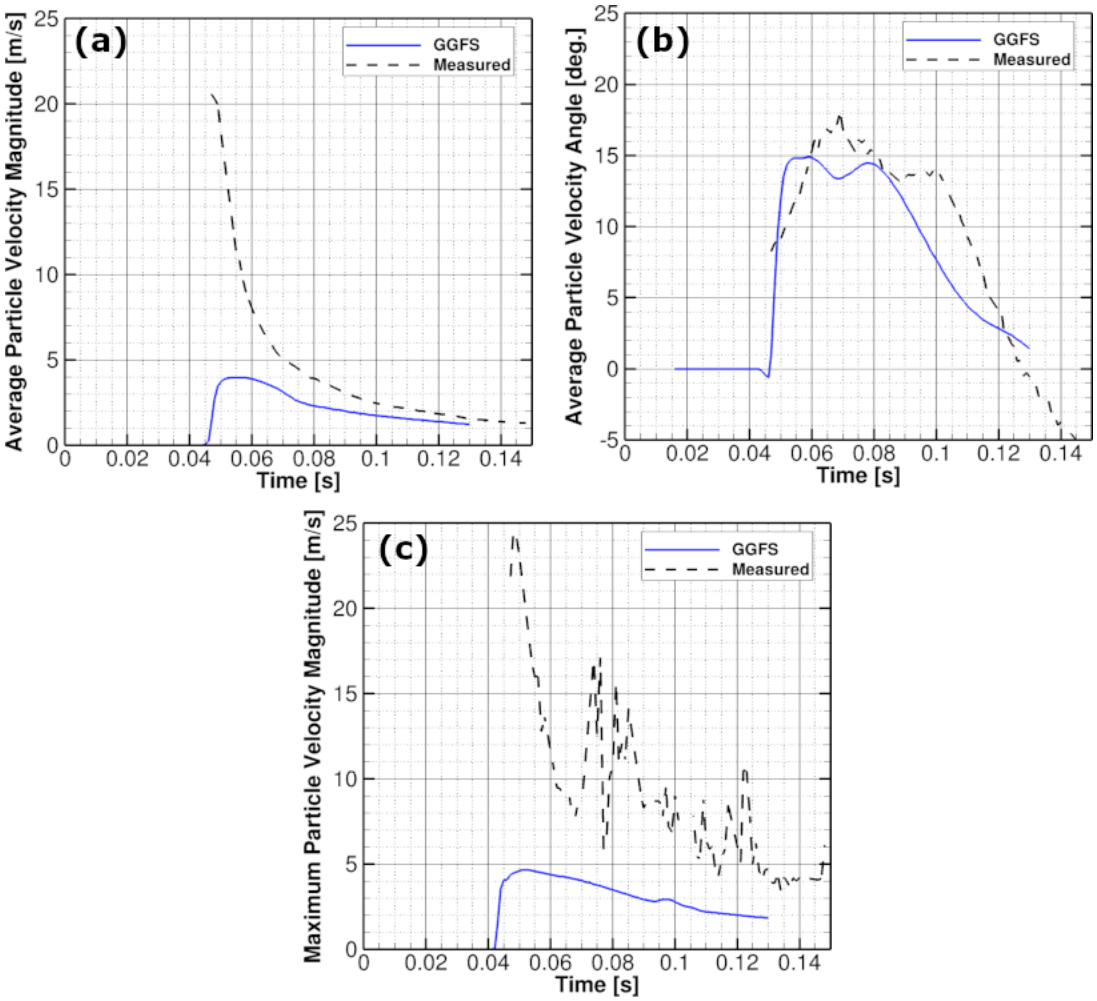

Fig. 12 Comparisons of particle velocities between Loci/GGFS and measurements from R142: (a) average velocity magnitude, (b) average velocity angle, and (c) maximum velocity magnitude

Loci/GGFS predictions of average and maximum velocity magnitudes follow a similar decay over time relative to measurements. Average velocity magnitudes are within 25% by 0.13 s, and maximum velocity magnitudes are within 60%. The data is much noisier for maximum velocity magnitudes than for average properties, and greater differences are observable between Loci/GGFS and measurements during the initial ejecta wave. The noisiness of the maximum particle velocity magnitudes and initial differences between Loci/GGFS and measurements are likely related.

It is likely that the initial differences between Loci/GGFS and measurements is due to insufficient modeling resolution in the Eulerian phase to capture the dilute ejecta and variations of a few particles at the extremes of the velocity distribution. The overall agreement is correspondingly improved as the ejecta crossing the field of view becomes much denser.

Lastly, good agreement in average velocity angles is evident from Fig. 12. The two-peaked profiles over time are consistent with the observations of two distinct ejecta waves. Moreover, both Loci/GGFS and experimental measurements show the same feature. Loci/GGFS predicts local maxima for each of these ejecta waves that are within 12% of measurements, and the trends are time are consistent with measurements.

B. R139

A much less violent cratering and ejecta process is observed for R139 relative to R142. The plume for R139 is also much more expanded than for R142. This can be observed from the Mach contours for the two selected cases in

Fig. 13. This is consistent with the identification of R142 as a deeper cratering, diffusion driven flow mechanism and R139 as a viscous shear erosion mechanism. Qualitative comparisons of observed ejecta will be made first in Figure Y and Z, followed by qualitative and quantitative comparisons of ejecta velocities.

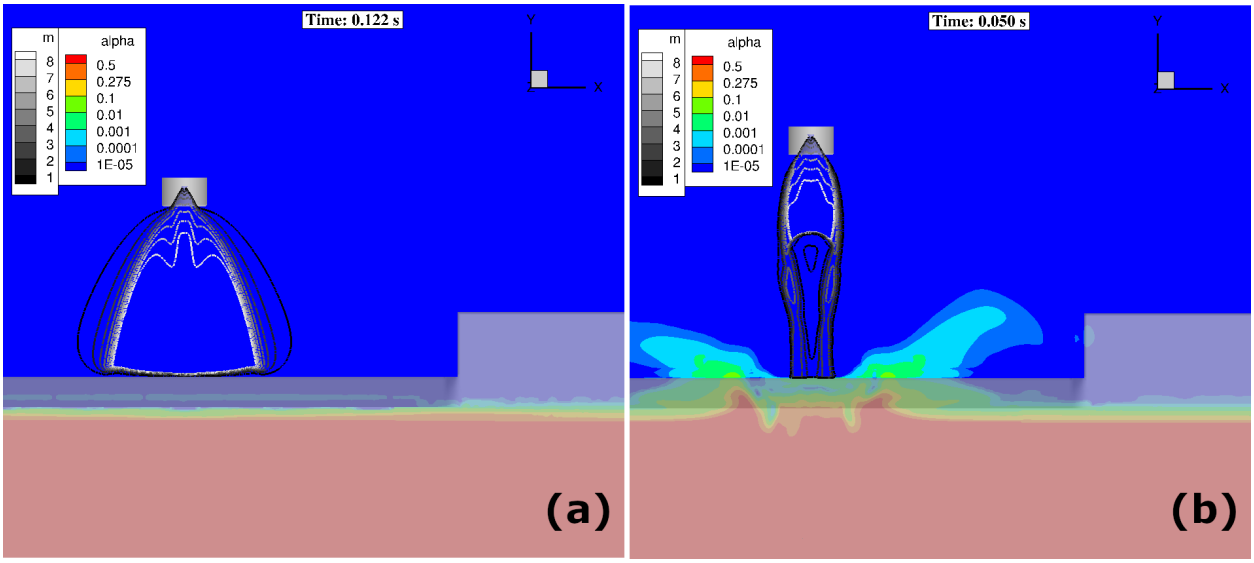

Fig. 13 Mach and solid volume fraction (alpha) contours near splitter plate for (a) R139 at 0.122 s and (b) R142 at 0.05 s

Fig. 14 shows Loci/GGFS predictions of solid volume fraction (alpha) on the left side and crater camera images on the right side for times from 0.12 s to 0.2 s. Images from the crater camera indicate a gradual increase in particle concentration towards the left side of the splitter plate over time, with only a few particles visible at 0.12 s. Solid volume fraction predictions from Loci/GGFS show a small streak of particles right along the surface up to 0.2 s. Loci/GGFS is not predicting the particles to be lifted as high as observed from the crater camera, but both exhibit erosion patterns consistent with viscous shear erosion.

After 0.3 s, Loci/GGFS predicts ejecta to flow radially outward that is mostly in line with the splitter plate. Some of the ejecta is also predicted to be slightly above the splitter plate on the left side. This can be observed from the images on the left side of Fig. 15. While the crater camera shows more particles reaching higher above the splitter plate relative to Loci/GGFS predictions, both indicate a significant portion of the ejecta traveling in line with the splitter plate.

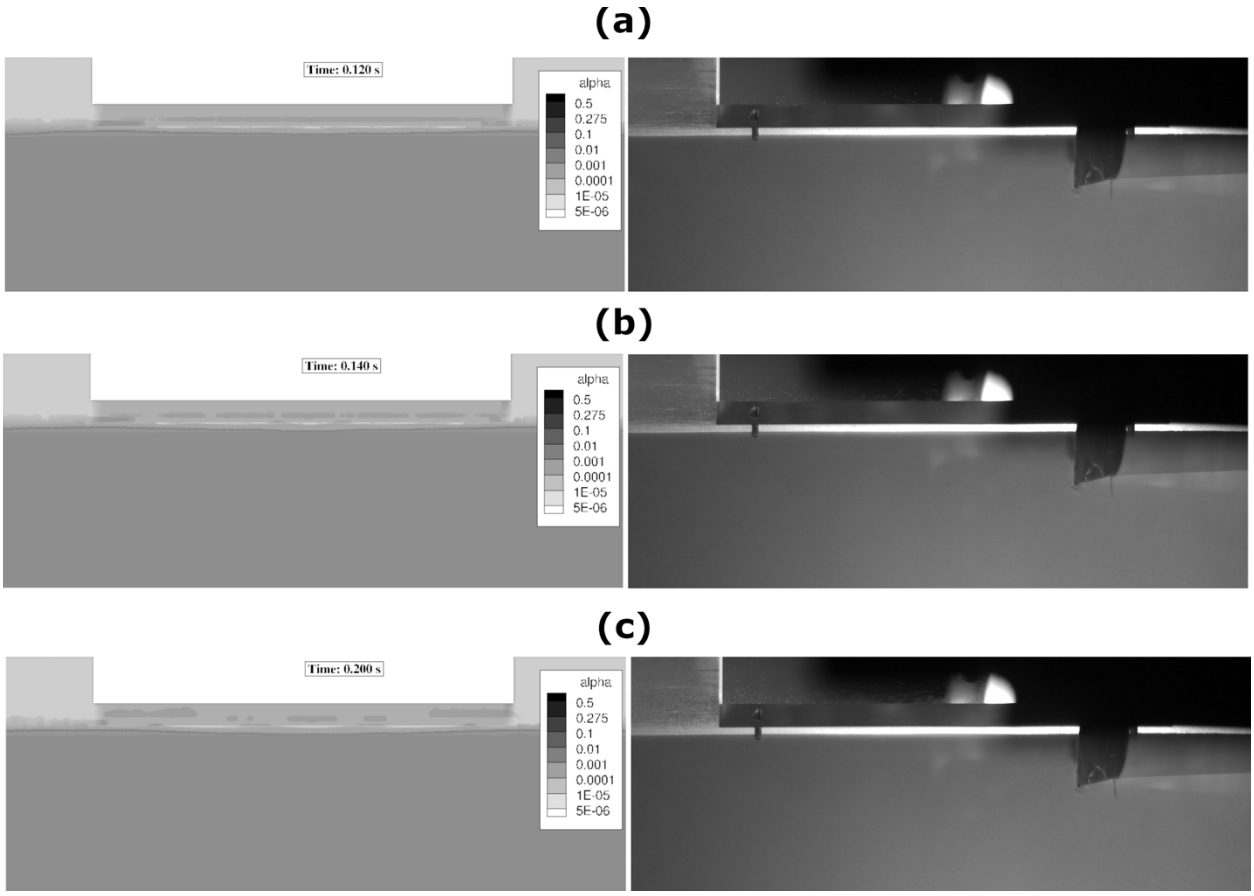

Fig. 14 Comparison of ejecta between Loci/GGFS (left images) and crater camera (right images) at times: (a) 0.12 s, (b) 0.14 s, (c) 0.2 s. Loci/GGFS images show alpha contours on slice near splitter plate

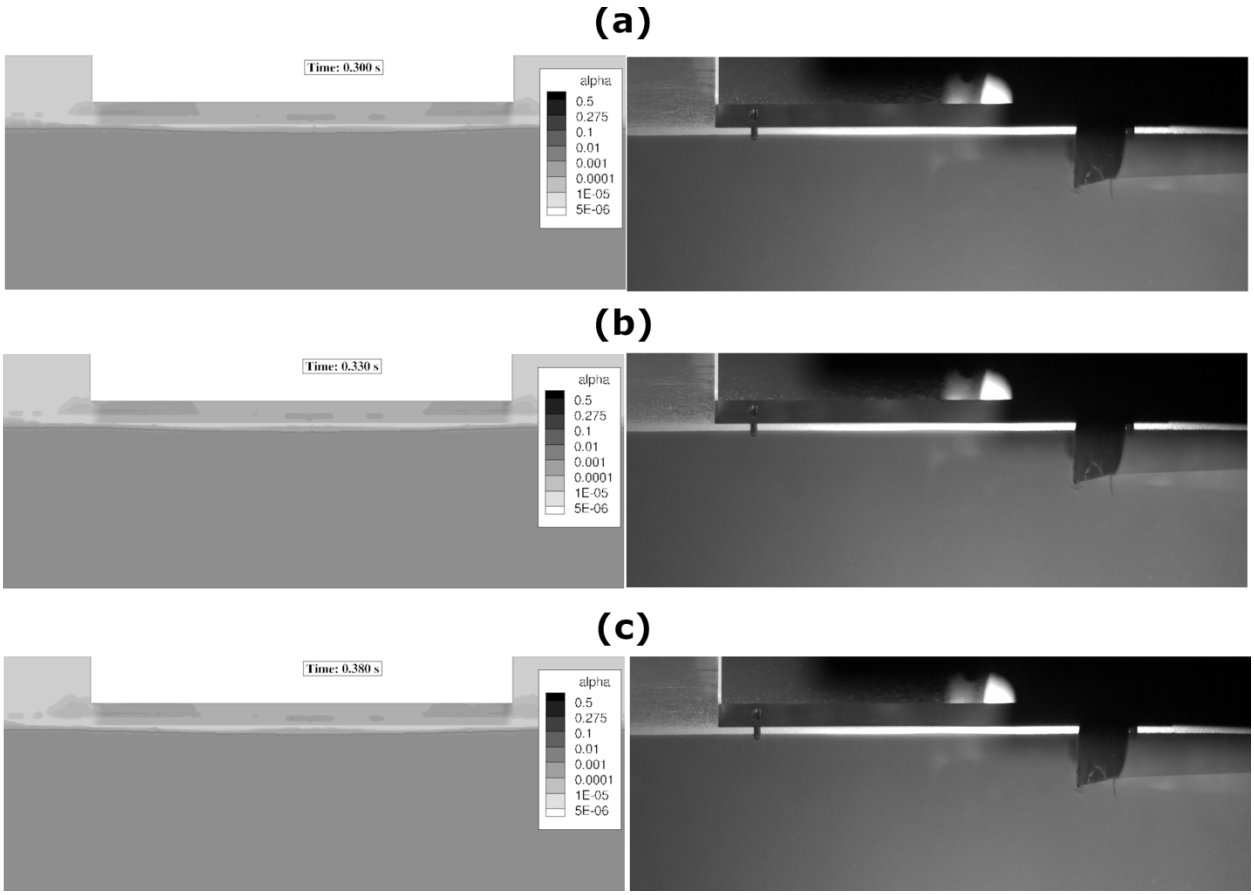

Fig. 15 Comparison of ejecta between Loci/GGFS (left images) and crater camera (right images) at times: (a) 0.3 s, (b) 0.33 s, (c) 0.38 s. Loci/GGFS images show alpha contours on slice near splitter plate

Average velocity magnitudes, average velocity angles, and maximum velocity magnitudes are shown as a function of time for both ejecta measurements and Loci/GGFS predictions in Fig. 16. The average velocities from measurements are obtained from Eq. (1) and average velocities from Loci/GGFS are obtained from Eq. (2).

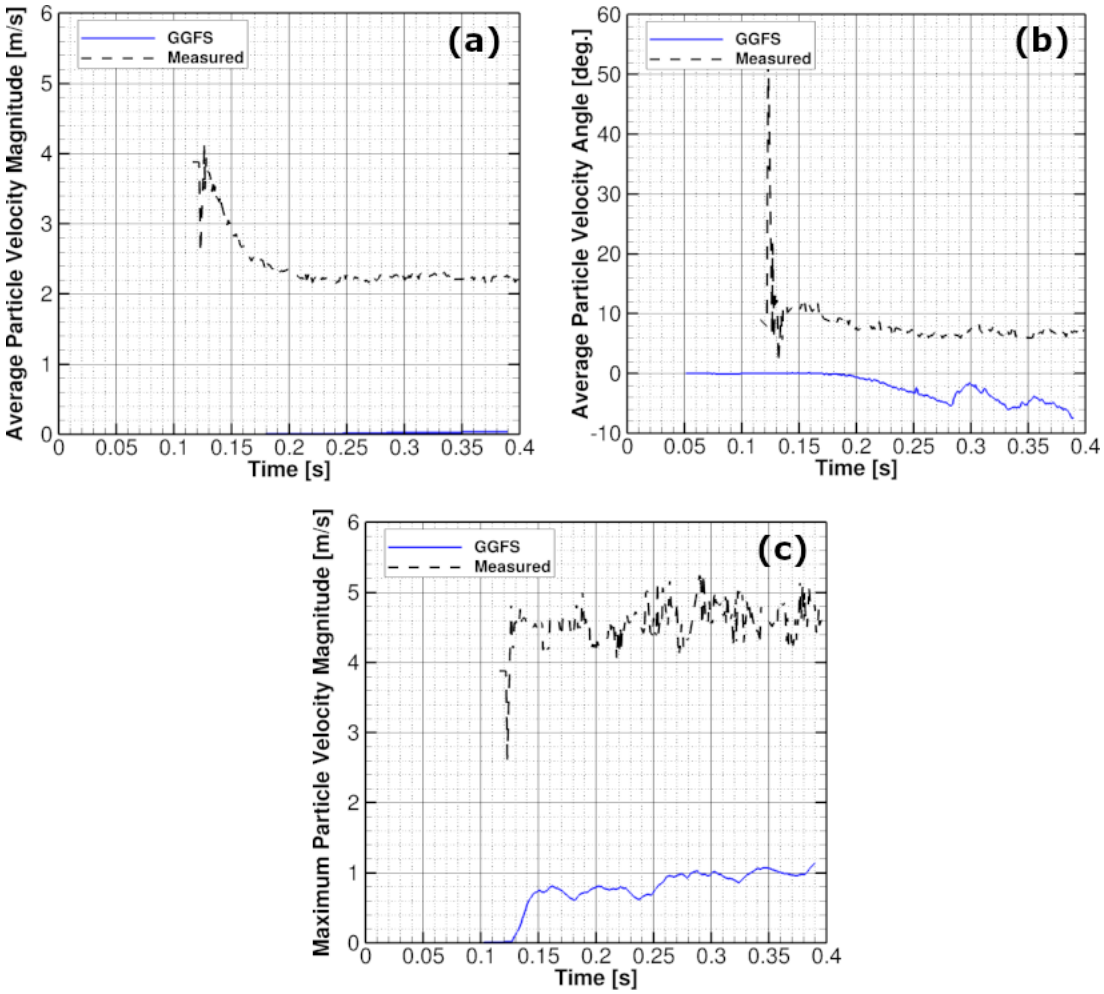

Fig. 16 Comparisons of particle velocities between Loci/GGFS and measurements from R139: (a) average velocity magnitude, (b) average velocity angle, and (c) maximum velocity magnitude

Loci/GGFS predictions of average and maximum velocity magnitudes gradually increase over time after approximately 0.15 s. Average and maximum velocity magnitudes from measurements are more constant over time after approximately 0.2 s and are significantly greater than those predicted from Loci/GGFS. Loci/GGFS average and maximum velocity magnitudes are two orders of magnitude and 75% less than measured, respectively.

Most of the ejecta from Loci/GGFS are predicted to be near the edge of the splitter plate, leaving much of the ejecta camera field of view with little-to-no ejecta. Also, the ejecta that is predicted from Loci/GGFS is mostly falling back down towards the surface within the ejecta camera field of view, resulting in negative average velocity angles. This is different from the measurements, which show a relatively uniform average velocity angle between six and eight degrees. This can be observed from Fig. 16.

Improved resolution of the gas/solid interface to lift individual solid particles (low solid volume fraction) may be needed to capture the ejecta in the dilute solid phase regime. With lower velocities predicted from Loci/GGFS, the particles do not travel as far and then mostly remain closer to the surface. This rationale for reduced predicted velocity magnitudes relative to measurements may also be applied to the average velocity angles.

VI. Discussion

The two validation experiments were purposely selected to assess the Loci/GGFS ability of capturing the ejecta particle phase velocity field for two extreme conditions: 1) a fluidized soil with deep cratering and large ejection of particle streams, and 2) a surface shear stress scouring only situation. The user has control over the proper physics resolution through two approaches: mesh resolution and physics model selection. The validation exercises contribute to developing guidance on modeling best practices on these options. They also serve to identify shortcomings and further refinements required in current physics model implementations which will provide guidance for the tool developers.

The shear stress scouring physics challenges the Eulerian two-fluid modeling approach ability to capture the surface shear erosion and resulting lofting of particle layers. The Eulerian volume-of-fluid representation does not directly identify a distinct interface surface but rather identifies gradients across the mesh cell. The high shear gradients may not be adequately resolved for the viscous shear erosion mechanisms in scouring mechanisms. Mesh size adequate for resolving high gradients must be set a-priori or through adaptive mesh refinement during a simulation. The scouring condition experiment simulation indicates that improved mesh resolution across the shear interface may be necessary to properly resolve the high gradients across a densely packed surface to capture proper shearing forces and resulting liberation and accelerations of particles from the soil surface.

The second issue arises from likely under-performance of the currently implemented gas-particle drag models derived from widely used Lagrangian particle models. These shortcomings have already been identified by the tool developers. The widely used models significantly underpredict the drag in the rarefied flow regime which may explain the particle velocity underprediction of the dilute ejecta.

The satisfactory Loci/GGFS performance for the highly fluidized cratering simulation indicates that the Eulerian modeling approach performed well for this situation with large volumes of fluidized ejecta being activated and accelerated. Underprediction of the particle velocities point again to the already identified shortcomings in the gas-particle drag model formulations.

Overall, the performed validations served to develop best practices for simulation setup such as mesh resolution and physics module selection. Identification and affirmation of already identified model improvements are required, most notably drag models. Establishing actual best practices and resolution requirements will be established in follow-on phase validations.

VII. Summary and Conclusions

A validation assessment has been performed for Loci/GGFS with respect to ejecta measurements from select PFGT1 tests. The two selected tests, R142 and R139, provided an assessment of ejecta predictions in the diffusion driven flow and viscous shear erosion cratering regimes, respectively. As a result of this validation assessment, predicted ejecta locations and velocities are compared over time with experimental measurements from the selected tests. The accuracy of the ejecta predictions from Loci/GGFS are evaluated and reported with respect to measurements.

It is found that the ejecta velocity predictions agree well with experimental measurements when and where the ejecta concentrations are greater. Thus, the agreement with measurements from a test with diffusion driven flow, R142, is better than for a test with viscous shear erosion, R139. Several key features from both selected tests are commonly predicted and observed between Loci/GGFS and test images. For example, both Loci/GGFS predictions and test images showed an initial wave of ejecta near the same point in time, followed by a second, denser wave of ejecta propagating radially outwards. Also, a similar splashing of dense ejecta against the splitter plate, resulting in a "V"-shaped ejecta pattern, is observed from Loci/GGFS predictions and test images. For R139, both Loci/GGFS predictions and test images show mostly surface scouring from a viscous shear erosion cratering process, albeit there are particles visible higher above the splitter plate in the test images relative to Loci/GGFS predictions.

Predicted average and maximum velocity magnitudes are within 25% and 60% of measurements, respectively, for R142. These differences are obtained at 0.13 s, noting that the trend is for improved agreement over time as the ejecta concentrations increase. Predicted average velocity angles for R142 also compare well with measurements over time and show similar two-peaked profiles corresponding to the observed two ejecta waves. The predicted local maxima for each of the two peaks in average velocity angles are within 12% of measurements, and both Loci/GGFS predictions and experimental measurements show a similar rise in velocity angle at the start of the test and decay in velocity angle towards of the end of the 0.13 s time frame.

Predicted average and maximum velocity magnitudes are two orders of magnitude and 75% less than measured from R139, respectively. Also, predicted average velocity angles tend to decrease over time (falling towards surface) rather than remain relatively constant over time at a positive value (lifting off surface). This test resulted in more

dilute ejecta and therefore poorer agreement with experimental measurements relative to R142. The poorer agreement is similar to the initial time frame from R142, when the ejecta were also more dilute. This supports the conclusion that more work needs to be done to improve modeling in the dilute phase. Thus, it is expected that improved resolution of the gas/solid interface causing individual particles to lift off the surface as well as the regions where those ejecta travel would lead to better agreement with experimental measurements.

References

[1] Gale, M., Buettner, K., Mehta, R., Liever, P. A., and Curtis, J., "Gas-Granular Flow Solver for Plume Surface Interaction and Cratering Simulations," AIAA Paper 2017-4503, *23rd AIAA Computational Fluid Dynamics Conference*, June 2017. doi: 10.2514/6.2017-4503

[2] Gale, M., Liever, P., Mehta, R., Yang J., and Curtis, J., "Realistic Regolith Models for Plume-Surface Interaction in Spacecraft Propulsive Landings," AIAA Paper 2020-0797, *AIAA SCITECH 2020 Forum,* 2020. doi: 10.2514/6.2020-0797

[3] Eberhart, C. J., West, J., and Korzun, A. M., "Overview of Plume-Surface Interaction Data from Subscale Inert Gas Testing at NASA MSFC Test Stand 300 Vacuum Facilities," AIAA Paper 2022-1811, *AIAA SCITECH 2022 Forum*, January 2020. Doi: 10.2514/6.2022-1811

[4] Korzun, A. M., Eberhart, C. J., West, J. S., Liever, P., Weaver, A. B., Mantovani, J. G., Langton, A. G., Kemmerer, B. W., and Atkins, A. R., "Design of a Subscale, Inert Gas Test for Plume-Surface Interactions in a Reduced Pressure Environment," AIAA Paper 2022-1808, *AIAA SCITECH 2022 Forum*, January 2022. doi: 10.2514/6.2022-1808

[5] Rubio, J. S., Gorman, M., Diaz-Lopez, M. X., and Ni, R., "Plume-Surface Interaction Physics Focused Ground Test 1: Setup and Preliminary Results," AIAA Paper 2022-1809, *AIAA SCITECH 2022 Forum*, January 2022. doi: 10.2514/6.2022-1809

[6] Rubio, J. S., Rodrigues, N. S., Diaz-Lopez, M. X., Gorman, M. T., and Ni, R., "Dynamics of Ejecta Produced by the Impingement of a Supersonic Jet," *J. Fluid Mech.*, 2024. (submitted)

[7] Lemmon, E. W., Bell, I. H., Huber, M. L, and McLinden, M. O, "Thermophysical Properties of Fluid Systems" in NIST Chemistry WebBook, NIST Standard Reference Database Number 69, Eds. P. J. Linstrom and W. G. Mallard, National Institute of Standards and Technology, Gaithersburg, MD, 20899, https://doi.org/10.18434/T4D303, (retrieved August 20, 2020)